Self-sustained divertor oscillations in ASDEX Upgrade

P. Heinrich[1,2], P. Manz[2,1], M. Bernert[2], G. Birkenmeier[2,1], D. Brida[2], M. Cavedon[2], P. David[2], M. Griener[2], G. Haas[2], T. Happel[2], U. Plank[2], F. Reimold[3], U. Stroth[2,1], M. Wischmeier[2], W. Zhang[2] and the ASDEX Upgrade Team[a]

[1] *Physik-Department E28, Technische Universität München, James-Franck-Str. 1, 85748 Garching, Germany*

[2] *Max-Planck-Institut für Plasmaphysik, Boltzmannstr. 2, 85748 Garching, Germany*

[3] *Max-Planck-Institut für Plasmaphysik, Wendelsteinstr. 1, 17491 Greifswald, Germany*

[a] *see the author list of H. Meyer et al. 2019 Nucl. Fusion 59 112014*

(Dated: July 1, 2020)

Alternating radiation phenomena between the inner and outer divertor regions in the sub kHz range are investigated in the tokamak ASDEX Upgrade. While the inner divertor oscillates between the onset and fluctuating state of detachment, the outer divertor oscillates between conditions where it can maintain high recycling conditions or not. The detachment state of the inner divertor determines the magnitude of the neutral flux through the private flux region, thus sets the recycling conditions at the outer divertor. In return these recycling conditions determine the particle content in the divertor, hence the detachment state at the inner divertor.

PACS numbers:

I. INTRODUCTION

The next generation magnetically confined fusion experiments like ITER and DEMO will exhibit a strong heat flux to the divertor tiles [1]. To prevent damage, a heat flux density of $\sim$16 MW m^{-2} should not be exceeded [2], which is aimed to be achieved by detachment [3, 4]. Fluid simulations are generally used to predict the behaviour of the divertor of future machines such as ITER or DEMO [5]. In these simulations it is often assumed that for steady-state input parameters, a unique steady-state solution will be reached. However, the equations describing the divertor plasma are complex and in general nonlinear [6] and therefore allow bifurcations or oscillations. A known example of such a nonlinear phenomenon in the divertor are *self-sustained divertor oscillations* (SSDOs) [7, 8]. Self-sustained divertor oscillations can occur at medium to high densities, with the heating power (maybe coincidental) close to the L-H transition threshold [7, 8]. The main feature is alternating D_α radiation from the inner and outer divertor regions in the sub kHz range. Reports show in JET a frequency around 8 Hz [7], in ASDEX Upgrade a frequency about 20–30 Hz [8, 9] and in H-mode plasmas in JET with ITER-like wall approximately 100 Hz [10]. These oscillations show a correlated increase in plasma edge density with a decrease in divertor neutral pressure, density, ion flux and radiation [7]. A minimum input power and a suitable density is required to observe this kind of oscillations [7]. These oscillations were predicted by Krasheninnikov et al. [6, 11, 12] and theoretically explained by bifurcations of the capability to maintain the recycling flux in high recycling conditions [6, 11, 12] as explained in more detail in Sec. III. Recent experiments [8] indicate that these oscillations are alternations between different states of detachment of the inner divertor as explained in more detail in Sec. II. In the present contribution the underlying mechanism for these divertor oscillations is investigated in the tokamak ASDEX Upgrade (AUG). In Sec. V it will be shown how the theory presented in Refs. [6, 11, 12] is connected to experimentally observed characteristics [8].

II. PREVIOUS FINDINGS

In a previous study in ASDEX Upgrade it has been found that the self-sustained divertor oscillations are alternations between two states of detachment [8], the *onset state* (OS) and the *fluctuating state of detachment* (FS), which are described in detail in Ref. [13] and introduced here in the following for convenience.

The typical magnetic field configuration is given by a forward field, *lower single null* (LSN) discharge, with the ∇B $\times$ B-drift directed towards the active X-point. Under attached conditions a strong asymmetric power distribution between both divertor targets is present with increased power loads on the outer divertor [14]. The reason are drifts in the *scrape-off layer* (SOL) and divertor region [14, 15]. The electron temperature gradient in the SOL creates a radial electrical field directed towards the wall elements $\mathrm{E_r} \sim -\nabla_r \mathrm{T_e}$. This drives a poloidal $\mathrm{E_r} \times$ B-flow from the inner towards the outer divertor in the main SOL resulting in a heat flux asymmetry between both divertor legs. The $\mathrm{E_r} \times$ B-flow transports charged particles from the outer to the inner divertor through the *private flux region* (PFR). The resulting enhanced density at the inner divertor facilitates the detachment of the inner divertor and reinforces low density, high temperature conditions in the outer divertor [16]. Furthermore a radial $\mathrm{E}_\theta \times$ B-drift in the divertor region transports charged particles across the strike line from the outer towards the inner divertor through the PFR [15]. As more power reaches the outer divertor, the inner divertor de-

taches first once a critical density in the divertor region is achieved. Recombination takes place in a thin layer close to the strike point of the inner target. On the *high field side* (HFS) a region of enhanced density called *high field side high density* (HFSHD) region is present below the X-point close to the strike point, with the HFSHD region as the main source of radiation. The position is a result of the divertor geometry. Most of the recycling neutral flux is released back to the *strike point region* (SPR) around the target normal, thus trapped within this region as the divertor tiles have a convex shape [13]. This state is referred to as the onset state of detachment. Increasing the density further, radiative oscillations are detected close to the X-point in the low kHz range [13, 17, 18]. Due to these so-called X-point oscillations this regime is called the fluctuating state of detachment [13]. The ionization region and the HFSHD region shift upstream towards the X-point. Subsequently the lower divertor segment is assumed to become transparent for neutrals and the released particles can travel through the PFR towards the *low field side* (LFS) [13]. The enhanced neutral flux from the inner to the outer divertor during this state will be of central importance for the here presented explanation of the SSDOs.

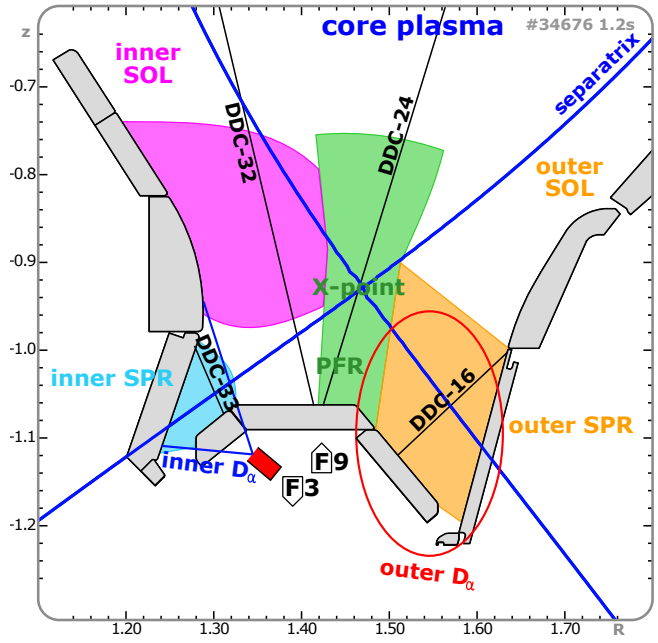

FIG. 1: The location of the pressure gauges (F and the arrow indicates the orientation) as well as the reference AXUV bolometric LOSs (labeled as "DDC") are shown. The colored areas correspond to the different regions in the divertor which show a different characteristic signal shape in the bolometric signals.

An alternating behavior between the onset state and the fluctuating state of detachment leads to an alternation of D_α radiation in the inner and outer divertor regions as explained in the following. At the HFS the HFSHD region is the most prominent source of radiation. During the OS, with the HFSHD region located close to the strike point region (partially inside the measurement cone) (Fig. 1), a higher level of (D_α) radiation is expected compared to the other states of detachment. At the outer divertor the opposite is expected. The neutral density in the outer divertor region as well as the radiation increases with increasing neutral flux through the private flux region during the early FS. While this explains why an alternating behavior between the OS and FS leads to the observed experimental signature of the SSDOs, it does not explain why these states alternate.

III. POSSIBLE CAUSE FOR SELF-SUSTAINED DIVERTOR OSCILLATIONS

A possible explanation for the cause of SSDOs is provided by Krasheninnikov et al. [6, 11, 12, 19] relating SSDOs to recycling driven bifurcations. At a certain critical input power the relation $T_\mathrm{d}(N_\mathrm{d})$ between the temperature at the divertor target T_d and total number of ions and neutral particles N_d in the corresponding flux tube becomes multivalued in some range of N_d, corresponding to a bifurcation of the plasma state (Fig. 2).

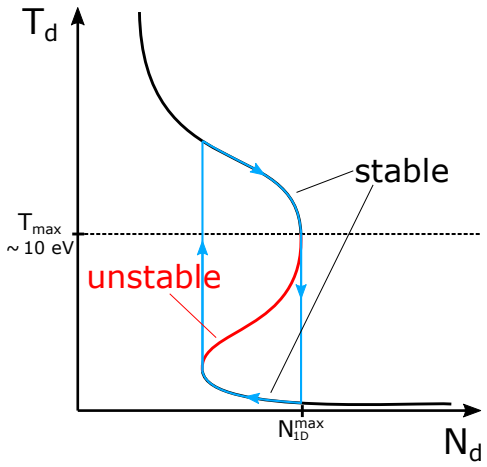

FIG. 2: Possible cause of the SSDOs adapted from Refs. [6, 12, 19]. N_d describes the particle content in the flux tube and consists of charged particles as well as neutrals. Around T_max the curve becomes multivalued, thus bifurcations can set in.

As the target temperature is above a critical threshold T_max ($T_\mathrm{d} \gtrsim 10$ eV) high recycling conditions can be sustained. The flux tube acts as a particle sink, thus is able to maintain a high neutral pressure. With increasing target density N_d the target temperature T_d decreases. If T_d drops below the critical value, all energy is spent for ionization and the energy flux into the recycling region is not high enough to support the plasma recycling flux [11, 12]. This leads to decreasing N_d together with T_d, correspond-

TABLE I: Global discharge parameters: magnetic field strength B_t, plasma current I_p, edge safety factor q_{95}, line averaged density $\overline{n_e}$ and auxiliary heating.

GLOBAL PARAMETERS						
shot#	gas	B_t [T]	I_p [MA]	q_{95}	$\overline{n_e}$ [m^{-3}]	heating [MW]
24664	D	−2.31	0.80	4.55	$5.59 \cdot 10^{19}$	1.32 (NBI)
27101	D	−2.52	1.00	4.10	$8.04 \cdot 10^{19}$	0.77 (ECRH)
29818	D	−2.48	1.00	4.07	$6.72 \cdot 10^{19}$	0.62 (ECRH)
29819	D	−2.48	1.00	4.14	$6.66 \cdot 10^{19}$	0.63 (ECRH)
29865	D	−2.49	1.00	4.13	$7.65 \cdot 10^{19}$	0.56 (ECRH)
34676	D	−2.49	0.80	5.01	$5.62 \cdot 10^{19}$	0.50 (ECRH)
						0.56 (ICRH)
34678	D	−2.49	0.80	5.01	$5.45 \cdot 10^{19}$	0.49 (ECRH)
						0.56 (ICRH)
35263	H	−2.47	0.80	5.06	$4.67 \cdot 10^{19}$	3.34 (NBI)
						0.46 (ECRH)

ing to a hump in $N_d(T_d)$ and a multivalued $T_d(N_d)$, which allows for bifurcations. As the high recycling conditions are no longer fulfilled particles leave the flux tube as the high neutral pressure cannot longer be maintained. Consequently for high temperatures ($T_d \gtrsim 10$ eV) the neutral flux can be directed towards the recycling region and for low temperatures ($T_d \lesssim 10$ eV) away from the recycling region [11, 12]. The neutral flux from one divertor to the other can lead to counter phase oscillations of both divertors, which periodically accumulate particles (ions and neutral particles) [6]. However, this assumes that both divertors are attached, which is experimentally not the case in AUG [8].

IV. DATA BASE AND DIAGNOSTICS

SSDOs appeared undesired in the presented data set of discharges. In some discharges SSDOs have even prevented reaching the foreseen research objective. No dedicated discharges have been performed. All of the discharges presented are forward field LSN discharges with the $\nabla B \times$ B-drift directed towards the active X-point. Global discharge parameters are shown in Tab. I. The magnetic field strength was close to $B = 2.5$ T, the plasma current was either 0.8 or 1 MA. Line averaged densities varied between $4.5 \cdot 10^{19} m^{-3}$ and $8.0 \cdot 10^{19} m^{-3}$. Self-sustained divertor oscillations have been identified by their main characteristic, the alternating behaviour of the D_α radiation between the inner and the outer divertor regions. The signals are derived from integrated radiation from Balmer-α transitions over a range of spectroscopic *lines of sights* (LOS) in the divertor region. In Fig. 1 the observed area is indicated in blue (inner D_α signal) and red (outer D_α signal). While the inner D_α radiation is measured close to the *inner strike point region* (iSPR) exclusively, the outer D_α radiation measurement covers a broader region. This includes the

TABLE II: Time when SSDOs occur (t_{DO}), number of SSDOs (#DO), duration of the OS (t_{OS}), duration of the FS (t_{FS}), their typical ratio (t_{OS}/t_{FS}) and the typical DO frequency f.

DIVERTOR OSCILLATION PARAMETERS						
shot#	t_{DO} [s]	#DO	t_{OS} [ms]	t_{FS} [ms]	t_{OS}/t_{FS}	f [Hz]
24664	2.1 – 3.8	21	37 – 71	10 – 92	0.84	12
27101	2.3 – 2.5	3	7 – 16	18 – 20	0.80	28
29818	1.7 – 3.4	10	22 – 34	85 – 148	0.21	7
29819	1.6 – 4.6	18 – 25	27 – 164	36 – 45	2.54	8
29865	2.5 – 2.8	4	17 – 27	18 – 43	0.86	19
34676	0.9 – 1.9	46 – 48	2 – 65	12 – 22	0.15	67
34678	1.1 – 1.7	8 – 12	4 – 23	25 – 221	0.18	30
35263	3.3 – 3.9	9	37 – 51	11 – 21	2.50	18
35263	5.2 – 6.2	18 – 20	12 – 34	8 – 61	0.94	30

outer strike point region (oSPR) as well as larger parts of the LFS divertor region and the private flux region. Its camera is directed in toroidal direction, therefore the measurement cone has an eliptical shape in the poloidal cross section. In addition the reference LOSs of the ***A****bsolute e****X****tended* ***U****ltra****V****iolet* (AXUV) bolometers and the positions of the *ASDEX pressure gauges* (APGs) are shown in Fig. 1. It is important to distinguish SSDOs from other low frequency oscillations. One example are sawteeth appearing in a similar frequency range, which can have a significant effect on the measured radiation in the divertor region. Sawteeth can be identified best in the soft X-ray emissions. If sawtheeth have been identified at the same frequency the discharges have been excluded from the data set.

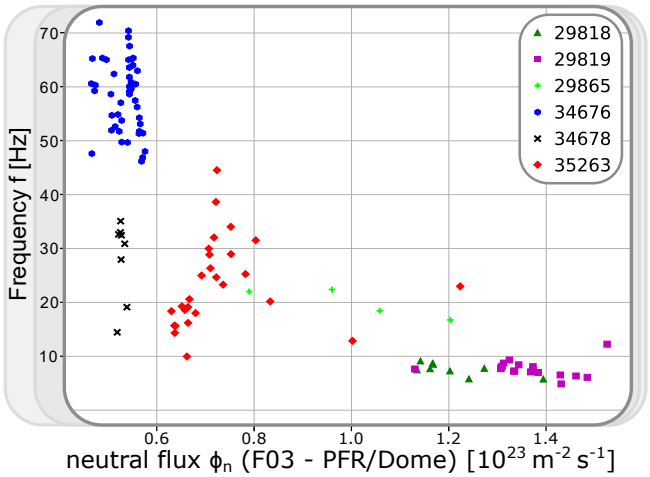

FIG. 3: Neutral flux in the private flux/dome region against SSDO frequency. No signal available for discharge #24664 and #27101. Only data points which are clearly identified as SSDOs are taken into account.

Frequencies from 7 up to 70 Hz have been observed in AUG (Tab. II). The frequency of the SSDOs seems to

decrease with line averaged density (measured in the center and the edge) and with the neutral flux in the private flux region indicated by different pressure gauges (Fig. 3). The APG F09 is directed towards the PFR through a small slit between the tiles. The pressure gauge F03 is used in Fig. 3 as F09 is not available for some of the discharges. The APG F03 measuring the neutral flux beneath the dome is used in order to have an extended data base. It shows the same trend as compared to F09. Additional information on how the flux measurement is performed is given in Ref. [20]. The arrow in Fig. 1 indicates the orientation of the APGs, with the tip representing its orientation.

For lower densities in the divertor region, this observed trend becomes less accurate. However, within the discharge #35263 the frequency seems to increase with increasing neutral flux. The highest frequency is observed in discharge #34676 heated by ICRH, which is known to enhance the impurity content in the discharge. The frequency in discharge #34676 is double the frequency of discharge #34678 at similar neutral flux and similar other parameters like magnetic field strength, density and heating powers.

All of the observed SSDOs so far are alternations between the OS and FS. In particular the FS is characterized by the appearance of radiative fluctuations at the X-point [13, 17], measured by AXUV bolometers, which display a high time resolution (sampling rate of 200 kHz) [21]. While the durations of the onset state t_{OS} and fluctuating state t_{FS} are often close to each other (in the previously reported discharges #27101 [8] and #29865 [9]), their duration can be strongly asymmetric. The discharges #29818 and #29819 are very similar with respect to the global discharge parameters and exhibit a similar frequency of the SSDOs, but are strongly asymmetric ($t_{\mathrm{OS}}/t_{\mathrm{FS}} = 0.21$ for #29818 and $t_{OS}/t_{FS} = 2.54$ for #29819).

V. DYNAMICS OF SELF-SUSTAINED DIVERTOR OSCILLATIONS

In this section the dynamics of the SSDOs are described. We choose discharge #29818, where the SSDOs exhibit a very low frequency around 7 Hz. This allows the study of slow evolution in more detail. The typical dynamics will be illustrated by two cycles of the SSDOs in Fig. 4. Except for 4c) the data has been averaged over several time points depending on the sampling rate of the diagnostic to remove frequencies above 1 kHz. A possible explanation for SSDOs is illustrated in Fig. 5. It will be referred to, while our physical interpretation of the measurements is explained.

The dynamics of the SSDOs can be split into two distinct time scales (Fig. 4). A slow, continuous evolution during the different states of detachment and fast bifurcations (indicated by the $\rightarrow$ symbol at the top in Fig. 4) at the transition from one state to the other. The changes on the slow time scale cause the bifurcations and determine the length of the individual onset and fluctuating state, thus set the frequency of the SSDOs. The dynamics of one cycle of a SSDO can be divided into four segments, the evolution during the onset and the fluctuating state, as well as the bifurcations between the OS and the FS (OS $\rightarrow$ FS and FS $\rightarrow$ OS respectively). In the following these phases are analyzed in more detail.

A. Evolution during the FS

The fluctuating state is defined by the occurrence of radiative fluctuations around the X-point. The radiation front propagates from below to above the X-point until it collapses and its propagation restarts from below the X-point [17]. Those X-point fluctuations occur with a typical frequency of 6 kHz [17] and they are observed in the spectrogram for the LOS DDC 24 directed towards the X-point (Fig. 4c). The average position of the ionization region is assumed to be located close to the X-point as indicated by the orange line in Fig. 5a. Thus, following Ref. [13] in the FS the private flux region should be transparent for neutrals (indicated by the light blue arrows in Fig. 5a). This should lead to an enhanced neutral flux through the PFR. Indeed a high neutral flux is measured by the divertor pressure gauges (Fig. 4d) during this state. In Fig. 4d the neutral flux is shown by the dashed lines, whereas the solid lines represent the data shifted by ~ 10 ms. This will be explained in detail in section V D. A beneficial effect of the neutral flux through the PFR on the development of the detachment has also been shown in SOLPS simulations [22]. Increased neutral flux from the inner towards the outer target has a cooling effect on the outer divertor region. This can be seen by a reduced temperature (Fig. 4f) and an increased radiation (Fig. 4a, b) at the outer target in the FS compared to the OS. In the FS, the electron temperature $\mathrm{T_e}$ of the outer divertor is below 10 eV (Fig. 4f) and at least the electron density is decreasing with decreasing electron temperature (Fig. 4f, g). However compared to the model by Krasheninnikov et al. [11, 12] (Fig. 2) this would indicate that the process follows the unstable branch. Here only the electron temperature and density at the target is measured, whereas in the model by Krasheninnikov et al. the trend for the overall density in the flux tube ($\mathrm{N_d}$) consisting of charged particles and neutrals is considered. As both density and temperature decrease, the plasma pressure decreases too. This pressure loss can be seen as a feature of detachment. In the model [11, 12] this state corresponds to the situation, where the energy flux into the recycling region cannot support the plasma recycling flux. As a consequence this region can act as a source for neutrals [11, 12], which can penetrate into the confined region and lead to fueling of the main plasma (indicated by the blue arrows from the outer target in Fig. 5a). Indeed, over the course of the FS, enhanced fueling of the main plasma is observed as shown by the line

averaged densities in the core (labeled as H1 in AUG) and edge (labeled as H5) (Fig. 4e). The fueling of the main plasma can be either from the LFS or the HFS. From the LFS this could be due to neutral fueling as explained in Refs. [11, 12] and also seen in modeling [23]. At the HFS during the FS, the HFSHD spends significant time well above the X-point [13, 17], which can also lead to enhanced plasma fueling [23, 24]. A reducing particle content in the divertor region over time is assumed as the gas puff for most of the examined discharges does not change in time and the density in the main plasma is increasing. This can be seen in the decreasing neutral flux (Fig. 4d) during the FS. The reduction of particle content in the divertor region is accompanied by another effect which is due to the partial detachment of the outer divertor. During the detachment process the ionization front at the oSPR shifts upstream and radially outwards, which is also indicated by observations of the bolometric signals at the outer divertor. In the plasma between the ionization front and the target plate, the temperature gradient along the field lines is reduced together with the strength of the $E_\theta \times$ B-drift. As a result the plasma particle flux from the outer towards the inner divertor through the PFR reduces. Due to the combination of the reduced particle flux from the PFR and the decreasing total particle density in the entire divertor volume (see above) also the ion flux Γ_{ion} in the inner SOL should be reduced. Also the power flux Q_H entering the inner SOL should be increased due to the reduced asymmetry by the decreasing strength of the $E_r \times$B-drift. Both, increasing power flux Q_H and decreasing ion flux Γ_{ion} should decrease the distance between the ionization front and inner divertor target (see Sec. V D for more details on the mechanism). A bifurcation-like transition into the onset state sets in, once this distance falls below a critical value (corresponding to a critical density and power threshold).

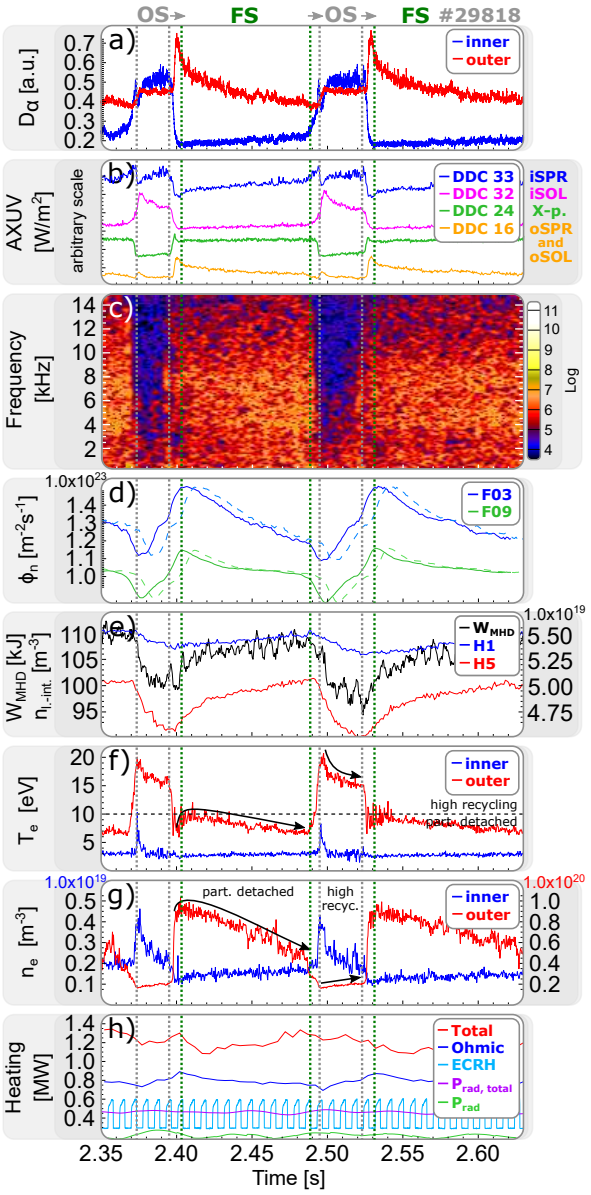

FIG. 4: Excerpt of time traces containing SSDOs from the discharge #29818. The bifurcations are indicated by $\rightarrow$ on the top. The time traces show the D_α radiation (a), AXUV radiation characteristics in (b) (reference LOSs shown in Fig. 1), the spectrogram at the X-point (c), neutral flux (d) (original data in dashed lines, solid lines shifted according to the explanations in Sec. V.D.), plasma stored energy W_{MHD}, central and edge line averaged density (labeled as H1 and H5) (e), electron temperature (f) and density (g) measured by Langmuir probes closest to the strike line and the heating power (h). Except for c) fluctuations above 1 kHz in the picture had been removed via averaging.

B. Bifurcation from the FS to the OS

Together with the transition from the fluctuating state towards the onset state the X-point fluctuations - which characterize the FS - vanish. This is also visible in the spectrogram in Fig. 4c) as the mode around 6 kHz ends during this time window. The radiation in the inner divertor enhances rapidly (Fig. 4a, b) as the HFSHD enters the measurement cone of the inner D_α-camera and inner target bolometric LOSs depicted in Fig. 1. The ionization front at the inner divertor is close to the target [13]. Most of the recycled flux gets absorbed at the ionization front and does not penetrate into the PFR (indicated by the light blue arrows in Fig. 5b). At the same time the lower divertor segment becomes opaque for neutrals, thus the neutral flux through the private flux region is further decreasing (Fig. 4d). As the cooling effect on the outer divertor ceases, the outer target temperature rapidly increases (Fig. 4f). The power distribution between both divertors depends on the $E_r \times$ B-drift, which is set by the radial temperature gradients. The outer target temperature gradient dominates as the inner divertor is in detached conditions. Assuming the temperature gradi-

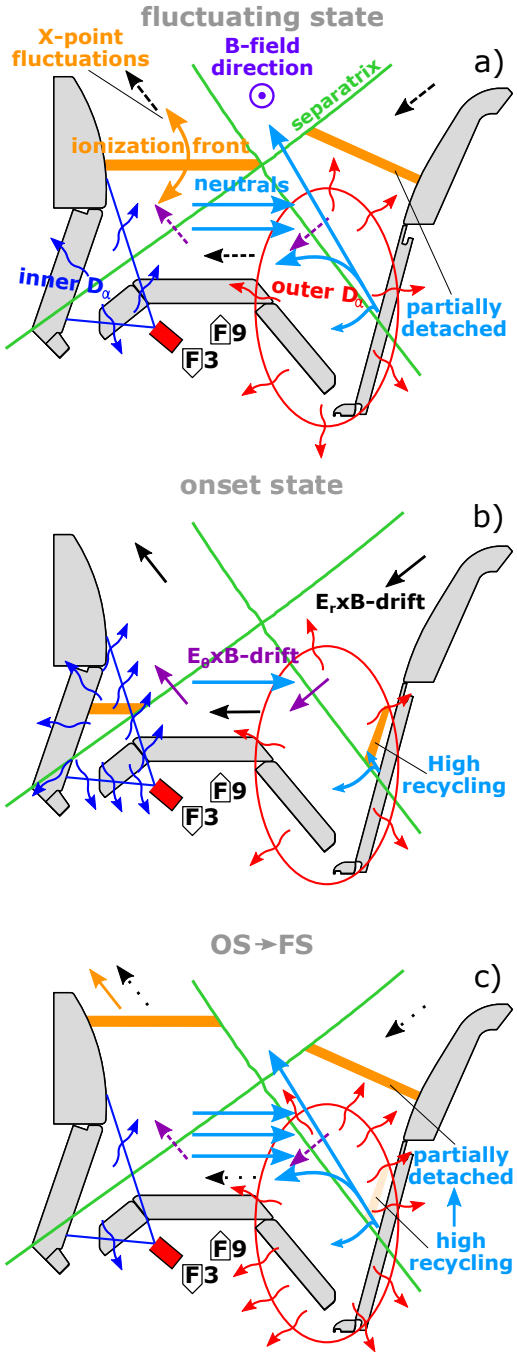

FIG. 5: Simplified model for the mechanism of the divertor oscillations. It shows the different states right at the beginning of each phase. A detailed explanation of the parameter evolution is given in the text.

ent fall-off length to stay rather constant, it mainly depends on the target temperature T_d of the outer divertor itself. Thus higher target temperatures ultimately lead to a stronger $E_r \times$ B-drift (indicated by the black arrows in Fig. 5b), hence a stronger asymmetry as more power reaches the outer divertor. The resulting stronger $E_r \times$ B-drift amplifies the temperature rise at the outer target as it further increases the asymmetry, hence the heat load towards the outer divertor. The outer target temperature increases by several eVs on a very short time scale during the FS → OS bifurcation, which is shown by the Langmuir probe measurements (Fig. 4f).

C. Evolution during the OS

In the onset state, the HFSHD region is located close to the inner target (indicated by the orange line in Fig. 5b) and the radiation at the X-point (Fig. 4b) is reduced. The radiation pattern is therefore opposite compared to the fluctuating state previously described, hence the characteristic alternation of the inner and outer D_α radiation is observed (Fig. 4a). During the OS, the outer divertor is in high recycling conditions as stated in Refs. [11, 12], at the target the temperature is well above 10 eV and plasma density is increasing with decreasing temperature (Fig. 2 and Fig. 4f, g). The (D_α) radiation (Fig. 4a, b) at the outer divertor is slightly elevated compared to the very end of the FS and the FS → OS bifurcation, which might be a signature of enhanced recycling processes at the outer divertor target (Fig. 4g). In the model described in Refs. [11, 12] the recycling region acts as a sink for neutrals and on the slow timescale the particle content in the divertor region can recover. Indeed, this can be seen in the neutral flux (Fig. 4d) and the plasma density at the outer target (Fig. 4g). Increasing plasma density in the divertor volume during the OS with the SSDOs have been reported before [9]. With recovering density (Fig. 4g) the temperature slowly decreases (Fig. 4f) as expected in the high recycling regime (Fig. 2). Also the fuelling of the confined plasma is reduced during the onset state, with the outer divertor being in high recycling conditions and the HFSHD region is located below the X-point, thus separated from the confined region. Hence the density in the confined region reduces (visible in line averaged core (H1) and edge (H5) densities in (Fig. 4e)) together with the confinement indicated by the plasma stored energy (W_{MHD} in Fig 4e)). The small variations on the W_{MHD}-signal coincide with the peaks of the pulsed ECRH heating scheme shown in Fig. 4h). For pulsed ECRH heating schemes the power deployed in the plasma can be determined via time averaging. The other power measurements for this particular discharge are also provided in Fig. 4h), but are not further discussed in detail as they vary between each discharge and depend on the individual operation itself. Additionally a slight reduction of the outer target temperature (Fig. 4f) during the OS results in a decreasing $E_r \times$ B-drift, hence a more evenly distributed power among both divertor targets and the particle flux towards the inner divertor via the $E_\theta \times$ B-drift also increases again. With recovering particle content the conditions slowly evolve back towards a situation where a transition into the fluctuation state becomes possible.

D. Bifurcation from the OS to the FS

The ionization region shifts upstream at the transition from the OS to the FS, with increasing density at the inner divertor or less power entering the inner divertor. This upwards shift with increasing density or decreasing power can be understood as follows [17, 25]. The inner divertor has to fulfill the energy balance $Q_H \approx \mathrm{E_{ion}}\Gamma_\mathrm{N}$, where Q_H is the power entering the SOL, $\mathrm{E_{ion}}$ the ionization cost and $\Gamma_\mathrm{N} \sim \sqrt{\mathrm{T}_b}/\Delta_b$. Here T_b is the inner divertor target temperature and Δ_b the distance between recombination and ionization front which can be approximated by the distance between target and ionization front [17]. With decreasing power Q_H reduces. In the high recycling regime the neutral flux Γ_N is equal to the ion flux Γ_ion to the target. Increasing the plasma density Γ_ion increases and with it also $\mathrm{E_{ion}}\Gamma_\mathrm{N} = \mathrm{E_{ion}}\Gamma_\mathrm{ion}$. This increase can be mediated by increasing the distance Δ_b with increasing plasma density such that $Q_H \approx \mathrm{E_{ion}}\Gamma_\mathrm{N} < \mathrm{E_{ion}}\Gamma_\mathrm{ion}$. In detached conditions, to compensate the lower power reaching the recombination region or an increase in density, Γ_N has to decrease, hence Δ_b has to increase [17, 25]. Therefore, the ionization front moves upstream with increasing density or decreasing power. This upstream shift has been observed in the LOSs directed towards the inner SOL region. By observation of the individual LOSs during this bifurcation a strongly radiating region shifts upstream over time. The radiation measured by each LOS increases first in the LOSs directed in the lower divertor segment followed by the LOSs in upstream direction with an increasing short time delay. At some point, the radiating region shifts above the X-point (indicated by the orange line in Fig. 5c). As it passes the LOS DDC 24 a small radiation peak can be observed (Fig. 4b). During this time no fluctuations at the low kHz range are observed, thus the typical X-point fluctuations did not set in until this point. Similar to the FS, the private flux region can be assumed to become transparent for neutrals again [13]. The neutral flux from the inner divertor may even be higher than in the subsequent FS, since the ionization front is assumed to be constantly above the X-point and not fluctuating in time (indicated by the multiple light blue arrows in Fig. 5c). Hence, the neutral flux rises to its maximum value (Fig. 4d). In the neutral flux measured by the pressure gauges in Fig. 4d, also two time scales can be identified. A rising interval corresponding to the time scale t_OS and a declining one corresponding to the time scale t_FS. This is observed for all discharges in the present data base. However, the neutral flux measured by the APGs appear to be delayed by $\sim$ 10 ms with respect to the appearance of the OS or FS, respectively. As this delayed response is not influenced by the variation in t_{OS} and t_{FS} in the data base, it can be concluded that the neutral flux measured by the APGs beneath the dome, is much likely delayed with respect to neutral dynamics below the X-point in the PFR. Such a delay in the response of the APGs has been previously observed during dynamic phenomena like ELMs in ASDEX Upgrade and DIII-D [26]. Here we assume that the neutral particles travel from the inner divertor through the PFR towards the outer divertor with their sound speed. The associated cooling effect on the outer divertor would be more or less instantaneous. During this time, only a few neutrals are detected by the APGs beneath the dome, as they do not directly measure the neutral flux inside the private flux region and multiple scattering is necessary to reach the pressure gauges. Neutrals can also be scattered at the plasma surface which has been shown in [27]. The neutrals which enter the LFS can be ionized there and cause the rapid increase in radiation (Fig. 4a, b), thus reduce the outer target temperature (Fig. 4f), while increasing the outer target plasma density (Fig. 4g). With a delay in the range of ms [26] the neutrals are released from the divertor plasma, thus the effect of the additional neutral flux towards the outer divertor is visible in the pressure gauges. This has been indicated by the blue arrows in Fig. 5a, c originating from the outer target. The signal in Fig. 4d has been shifted by $\sim$ 10 ms to indicate how the neutral flux through the PFR might look like, as this is of interest in the present study.

With the temperature dropping below 10 eV the outer divertor transits into the state, where the energy flux into the recycling region cannot sustain the plasma recycling process [11, 12], thus partially detaches again.
At the inner target the upstream shifting ionization front enters the shadow of the divertor nose where it cannot be supplied by the neutral flux from the recombination region close to the inner strike point as shown in [17]. The radiating region collapses to a position below the X-point and from there shifts upstream again passing the LOSs in the divertor region and is visible as the frequency band around 6 kHz. These cyclic reformations of the radiation front propagating from below to above the X-point are a signature of the X-point fluctuations defining the FS [17]. The initial situation (FS) at the beginning of the SSDO is reestablished and the cycle can repeat.

VI. SUMMARY, DISCUSSION AND CONCLUSION

All discharges analyzed so far are consistent with the previous finding of Potzel et al. [8] that divertor oscillations are alternations between two states of detachment, the onset state and the fluctuating state of detachment [13]. These states concern mainly the region of the inner divertor. The outer divertor seems to bifurcate between high recycling and partially detached conditions, whereby a recycling capability of the divertor has been proposed by Krasheninnikov [11, 12] to be cause of the self-sustained divertor oscillations (Fig. 2).
Divertor oscillations exhibit two time scales, a slow continuous evolution during different states of detachment

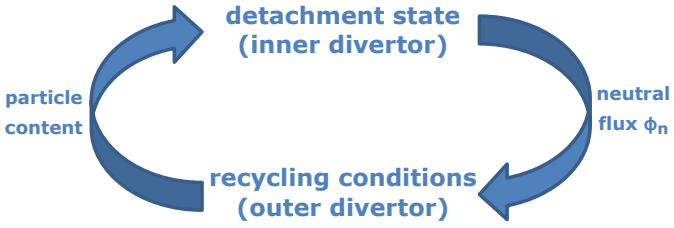

FIG. 6: Simplified cycle of the SSDOs. It shows how the conditions of the inner and outer divertor affect each other during the process.

and bifurcations at the transitions from one state to the other. The fast time scale seems to be set by the neutral flux from the inner to the outer target. The neutral flux to the outer divertor itself depends on the state of detachment of the inner divertor (Fig. 6). The long time scale seems to be set by the fueling of the main plasma, which is determined by the recycling conditions at the outer divertor. The fueling determines the particle content in the divertor and sets the detachment state (Fig. 6). While the inner divertor is in the fluctuating state of detachment, the outer divertor cannot maintain high recycling conditions, thus partially detaches. This can be seen by decreasing plasma density (Fig. 4g) and neutral flux (Fig. 4d) with decreasing target temperature (Fig. 4f). As a result neutrals are leaving the recycling region and the particle content in the divertor volume decreases. At some point the particle content and the power distribution between the divertor halves lead to a transition of the inner divertor from the fluctuating state to the onset state of detachment. In the fluctuating state the private flux region is assumed to be transparent for neutrals [13] cooling the outer divertor, whereas in the onset state the private flux region is opaque for neutrals. The suddenly reduced neutral flux to the outer divertor results in a strong temperature increase, which is further amplified by the $E_r \times B$-drift modifying the asymmetry of the power flux towards the outer divertor. At the resulting elevated temperatures the outer divertor can operate in high recycling conditions again. Therefore, in the onset state the particle content in the divertor recovers. The plasma density at the inner divertor can increase also due to the enhanced $E \times B$-drifts from the outer divertor through the private flux region. With increasing plasma density at the inner divertor or reduced power entering the inner divertor half, the ionization front moves upstream while a transition into the fluctuating state of detachment takes place. The cycle can repeat.

Self-sustained divertor oscillations as studied in the present contribution are rather annoying than dangerous. The observed oscillations appear in L-mode conditions with the outer divertor target around the detachment conditions.

On the other hand, a fusion reactor is foreseen to operate in detached H-mode conditions. Stable completely detached H-mode plasmas have been demonstrated in ASDEX Upgrade with the help of impurity seeding [28, 29]. In those discharges SSDOs have not been observed so far, also because in those discharges edge localised modes (ELMs) appear, preventing the SSDOs. However similar oscillations had been observed in JET with an ITER-like wall also during H-mode [10] and have been related to *impurity induced divertor oscillations* [12, 19, 30, 31]. In ITER plasma simulations impurity driven self-sustained divertor oscillations result in a significant modulation in the divertor heat load ($\sim$ 30 %) [12, 19]. To provide a safe operation for future devices such as ITER, this kind of oscillations should therefore be studied in ELM-free, detached H-mode conditions.

As neutral particle dynamics seems to be the driver for the SSDOs explained in the present contribution - and most of the here discussed effects are taken into account in SOLPS - SOLPS simulations similar to the ones presented in Ref. [6] at AUG conditions would be desirable. In particular the role of the neutral flux through the PFR should be investigated in more detail. For AUG the database has to be extended to identify critical parameter thresholds. Until now no dedicated discharges to study the divertor oscillations had been performed in AUG. The impact of the magnetic configuration and divertor structure on this phenomenon would be also a desirable subject for further investigations.

Acknowledgements

The authors thank the anonymous referees for their constructive comments significantly improving this manuscript.

This work has been carried out within the framework of the EUROfusion Consortium and has received funding from the Euratom research and training programme 2014-2018 and 2019-2020 under grant agreement No 633053. The views and opinions expressed herein do not necessarily reflect those of the European Commission.

[1] T. Eich, A. W. Leonard, R. A. Pitts, W. Fundamenski, R. J. Goldston, T. K. Gray, A. Herrmann, A. Kirk, A. Kallenbach, O. Kardaun, et al., Nucl. Fusion **53**, 093031 (2013).

[2] R. A. Pitts, X. Bonnin, F. Escourbiac, H. Frerichs, J. P. Gunn, T. Hirai, A. S. Kukushkin, E. Kaveeva, M. A. Miller, D. Moulton, et al., Nuclear Materials and Energy **20**, 100696 (2019).

[3] H. Zohm, C. Angioni, E. Fable, G. Federici, G. Gantenbein, T. Hartmann, K. Lackner, E. Poli, L. Porte, O. Sauter, et al., Nucl. Fusion **53**, 073019 (2013).

[4] A. Loarte, J. W. Hughes, M. L. Reinke, J. L. Terry,

B. LaBombard, D. Brunner, M. Greenwald, B. Lipschultz, Y. Ma, S. Wukitch, et al., Physics of Plasmas **18**, 056105 (2011).
[5] S. Wiesen, D. Reiter, V. Kotov, M. Baelmans, W. Dekeyser, A. S. Kukushkin, S. W. Lisgo, R. A. Pitts, V. Rozhansky, G. Saibene, et al., Journal of Nuclear Materials **463**, 480 (2015).
[6] A. S. Kukushkin and S. I. Krasheninnikov, Plasma Physics and Controlled Fusion **61**, 074001 (2019).
[7] A. Loarte, R. D. Monk, A. S. Kukushkin, E. Righi, D. J. Campbell, G. D. Conway, and C. F. Maggi, Physical Review Letters **83**, 3657 (1999).
[8] S. Potzel, M. Wischmeier, M. Bernert, R. Dux, H. W. Müller, and A. Scarabosio, Journal of Nuclear Materials **438**, S285 (2013).
[9] L. Guimarais, S. Potzel, C. Silva, M. Bernert, D. Carralero, G. D. Conway, L. Gil, M. E. Manso, V. Nikolaeva, F. Reimold, et al., Nucl. Fusion **58**, 026005 (2018).
[10] A. R. Field, I. Balboa, P. Drewelow, J. Flanagan, C. Guillemaut, J. R. Harrison, A. Huber, V. Huber, B. Lipschultz, G. Matthews, et al., Plasma Phys. Control. Fusion **59**, 095003 (2017).
[11] S. I. Krasheninnikov, A. S. Kukushkin, V. Pistunovich, and V. A. Pozharov, Nucl. Fusion **27**, 1805 (1987).
[12] S. I. Krasheninnikov, A. S. Kukushkin, and A. A. Pshenov, Physics of Plasmas **23**, 055602 (2016).
[13] S. Potzel, M. Wischmeier, M. Bernert, R. Dux, H. W. Müller, A. Scarabosio, and the ASDEX Upgrade Team, Nucl. Fusion **54**, 013001 (2014).
[14] L. Aho-Mantila, S. Potzel, D. P. Coster, M. Wischmeier, M. Brix, R. Fischer, S. Marsen, A. Meigs, H. W. Müller, A. Scarabosio, et al., Plasma Phys. Control. Fusion **59**, 035003 (2017).
[15] P. C. Stangeby, *The Plasma Boundary of Magnetic Fusion Devices* (Institute of Physics, Bristol, Philadelphia, 2000).
[16] A. E. Jaervinen, S. L. Allen, D. Eldon, M. E. Fenstermacher, M. Groth, D. N. Hill, A. W. Leonard, A. G. McLean, G. D. Porter, T. D. Rognlien, et al., Physical Review Letters **121**, 075001 (2018).
[17] P. Manz, S. Potzel, F. Reimold, M. Wischmeier, and the ASDEX Upgrade Team, Nuclear Materials and Energy **12**, 1152 (2017).
[18] S. I. Krasheninnikov and A. I. Smolyakov, Physics of Plasmas **23**, 092505 (2016).
[19] R. D. Smirnov, A. S. Kukushkin, S. I. Krasheninnikov, A. Y. Pigarov, and T. D. Rognlien, Physics of Plasmas **23**, 012503 (2016).
[20] G. Haas and H. S. Bosch, Vacuum **51**, 39 (1998).
[21] M. Bernert, T. Eich, A. Burkhart, J. C. Fuchs, L. Giannone, A. Kallenbach, R. M. McDermott, B. Sieglin, and the ASDEX Upgrade Team, Review of Scientific Instruments **85**, 033503 (2014).
[22] A. A. Pshenov, A. S. Kukushkin, and S. I. Krasheninnikov, Physics of Plasmas **24**, 072508 (2017).
[23] F. Reimold, M. Wischmeier, M. Bernert, M. Dunne, S. Potzel, L. Guimarais, T. Lunt, D. Reiter, the ASDEX Upgrade Team, and the EUROfusion MST1 Team, Nuclear Materials and Energy **12**, 193 (2017).
[24] M. G. Dunne, S. Potzel, F. Reimold, M. Wischmeier, E. Wolfrum, L. Frassinetti, M. Beurskens, P. Bilkova, M. Cavedon, R. Fischer, et al., Plasma Phys. Control. Fusion **59**, 014017 (2017).
[25] S. I. Krasheninnikov, M. Rensink, T. D. Rognlien, A. S. Kukushkin, J. A. Goetz, B. LaBombard, B. Lipschultz, J. L. Terry, and M. Umansky, Journal of Nuclear Materials **266-269**, 251 (1999).
[26] G. Haas, R. Maingi, and J. Neuhauser, Journal of Nuclear Materials **266–269**, 1065 (1999).
[27] G. Haas, P. Bachmann, D. Düchs, R. Reichle, D. Reiter, and R. Schneider, Journal of Nuclear Materials **196–198**, 481 (1992).
[28] F. Reimold, M. Wischmeier, M. Bernert, S. Potzel, A. Kallenbach, H. W. Müller, B. Sieglin, U. Stroth, and the ASDEX Upgrade Team, Nucl. Fusion **55**, 033004 (2015).
[29] A. Kallenbach, M. Bernert, M. Beurskens, L. Casali, M. Dunne, T. Eich, L. Giannone, A. Herrmann, M. Maraschek, S. Potzel, et al., Nucl. Fusion **55**, 053026 (2015).
[30] P. Bachmann, D. Sünder, and U. Wenzel, Contributions to Plasma Physics **36**, 519 (1996).
[31] J. Neuhauser, W. Schneider, and R. Wunderlich, Nuclear Fusion **26**, 1679 (1986).